

Self-folding mobile microrobots for biomedical applications

Stefano Fusco¹, Mahmut Selman Sakar¹, Stephen Kennedy², Christian Peters³, Salvador Pane¹, David Mooney², and Bradley J. Nelson¹

Abstract—The presented microrobotic platform combines the advantages of self-folding NIR light sensitive polymer bilayers, magnetic alginate microbeads, and a 3D manipulation system and introduces a solution for targeted, on-demand drug and cell delivery. First feasibility studies are presented together with the potential of the full design.

I. INTRODUCTION

In recent years, several miniaturized devices were developed for minimally invasive interventions. They can potentially increase the quality and the efficiency of surgeries or therapies, minimizing at the same time the risks and the pain for the patients [1]. One successful example is the Pillcam, a centimeter scale pill-sized wireless camera developed for performing endoscopy in the gastrointestinal tract. The ability to guide untethered microtools inside the human body to target locations is an important feature and wireless magnetic manipulation offers great promise [2], [3]. Several groups demonstrated magnetic steering of microrobots *in vivo* for ophthalmic interventions [4], biopsy [5], and cancer therapy [6].

It is highly desirable to trigger and/or regulate the functionality of individual or groups of magnetic microrobots with external cues for spatiotemporally controlled delivery of biological agents (e.g., drugs and cells). Dynamical control over delivery can potentially improve the efficiency of the agents, and permit new therapies. In this work, we introduce externally triggered soft-bodied mobile microrobots for on-demand cell and drug delivery. The overall concept is summarized in Figure 1. The soft body of the microrobot would permit adaptive and safe maneuvering inside target organs and cavities.

We fabricated hydrogel bilayers with bioinspired morphologies (Jellyfish or Venus Flytrap) using conventional 2D photolithography. A double step process was used to couple a graphene oxide nanocomposite of a highly swelling thermoresponsive hydrogel layer (based on N-isopropylacrylamide, NIPAAm), with a layer of polyethylenglycol-diacyrlyate (PEGDA). Different expansion properties of layers results in an inhomogeneous expansion/shrinking along a certain direction which leads to self-folding (see Figure 2). The devices have switchable and

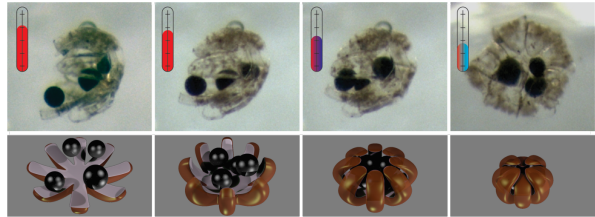


Fig. 1. Principle of photoactivatable magnetic microrobots. An increase of temperature allows the controlled encapsulation and release of cell laden magnetic microbeads. The full platform is then magnetically steered to the target location and actuated by NIR light (induces heating) to deliver the payload.

reversible properties and can perform on-demand tasks as the transition can be controlled by external stimuli [7], [8].

The first layer was specifically designed to collapse at temperatures higher than 40°C or by short exposure to a NIR laser source. The second and passive layer was used to achieve complete folding of the final structures upon immersion into water. As a result, the microstructures can encapsulate and protect magnetic alginate microbeads in their folded state. The bead-carrying microrobots were steered by means of a 5-DOF electromagnetic manipulation system [9]. They were actuated by short exposure to a NIR laser source, which led to the release of the encapsulated microbeads and the modification of the drug release from the bilayers.

II. MATERIALS AND METHODS

A. Fabrication of Hydrogel Bilayers

The microdevices are the result of a double photolithographic process [10], where the different layers are subsequently created, without any alignment, by backside exposure on a glass photomask (Figure 3). The hydrogel solutions were inserted by means of capillary forces in between the mask, and a bottom silicon substrate, with SU-8 spacers of defined thickness. The shape of the structures were designed to form closed compartments after self-folding.

The masks were printed on plastic foil (Selba S.A, Switzerland) and reproduced on glass wafers by photolithography using the photoresist AZ4562. A 100 nm chromium layer was subsequently evaporated on the substrates, and removed from the featured areas by dissolving the photoresist in acetone and isopropanol. The final masks were then coated with a lift off sacrificial adhesive layer to provide uniform adhesion of the hydrogel layers. SU-8 spacers of different thicknesses (from 10 to 40 μm) were prepared by photolithography on SiO₂ substrates. A non adhesive silane

¹Institute of Robotics and Intelligent Systems, ETH Zurich, 8092 Zurich, Switzerland. email: sakarm@ethz.ch

²Wyss Institute of Biologically Inspired Engineering, Harvard University, Cambridge, MA 02138, USA

³Institute of Micro and Nanosystems, ETH Zurich, 8092 Zurich, Switzerland

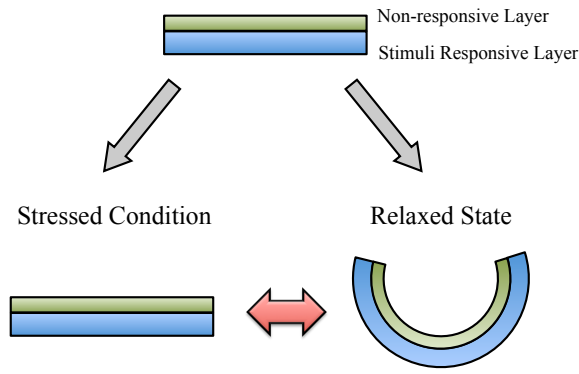


Fig. 2. Folding of 2D thin films happens as a result of an inhomogeneous expansion/shrinking along a certain direction. This can be achieved by coupling two layers with different expansion properties. Moreover, if one of these layers undergoes active or controlled shape transition, this would result in a controlled folding/unfolding mechanism.

layer (PFDTCS, Sigma Aldrich, USA) was added by vapor deposition to prevent hydrogel adhesion on this side of the chamber.

After placing the mask on the spacer substrate, a first hydrogel solution, based on PEGDA (3 wt% DMPA photo initiator, 50 wt% ethyl lactate solvent. All materials were purchased from Sigma Aldrich, USA) was infiltrated into the photo polymerization cell (defined thickness, 10 μm) and polymerized at 365 nm for 2 minutes (Karl Sss Microtec, 300 W mercury lamp, Germany). After separating the two substrates, the polymerized hydrogel features remained on the glass mask.

The NIR light responsive hydrogel layer was composed of NIPAAm, acrylamide and PEGDA as a crosslinker (NIPAAm-AAm-PEGDA molar ratio 85/15/0.5, 3 wt% DMPA photo initiator, 70 wt% ethyl lactate, all materials purchased from Sigma Aldrich, USA). A 3 wt% graphene oxide, produced by controlled oxidation from graphite was added and dispersed into the hydrogel solution by ultrasonication (4000 J, probe sonicator, SONICS, USA). The solution was introduced into the space between the photo mask and another substrate, after removing the previously unpolymerized solution. A thicker spacer (40 μm) was used in this case, and the polymerization was carried out for an additional three minutes. Afterwards, the samples were released by simple immersion in water and rinsed deeply to remove the unreacted materials.

B. Fabrication of Alginate Microbeads

Magnetic microbeads were formed by nebulization from a mixture of alginate (LF10/60, LF20/40, Sigma Aldrich), iron oxide and phosphate buffer saline (PBS) into a bath of calcium chloride. The alginate was first dissolved into deionized water, and after various sterilization and liophilization treatments, dissolved again in PBS (2.5 wt% using a ratio of 4:1 LF10/60: LF20/40) and mixed with 100 mg/ml iron(III) oxide powder ($< 5\mu\text{m}$ diameter, Sigma Aldrich). The mixture was then nebulized over a 100 mM calcium chloride bath (flow at 3.13 ml/min, volumetric flow rate of 30 cubic

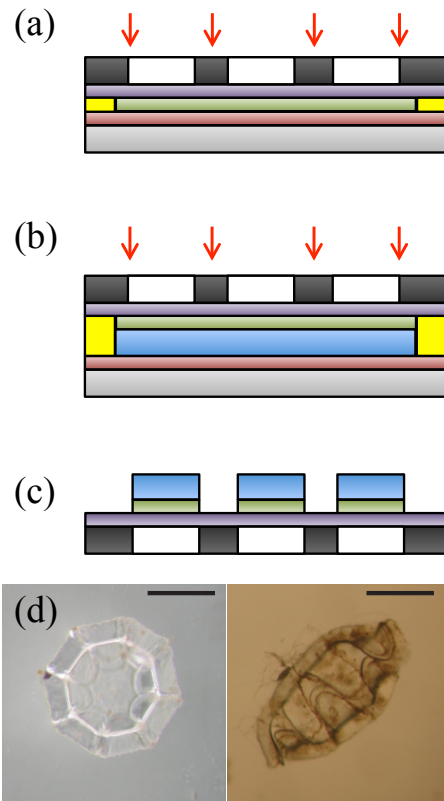


Fig. 3. Fabrication method of the hydrogel bilayers. A) The non-responsive layer (green) is polymerized upon UV exposure on the photomask, due to the selective coating of adhesive (purple) and non-adhesive layers (red). B) In the second step, the thermoresponsive layer (blue) is polymerized on the bottom of the first layer using a thicker spacer substrate (yellow). c) The two layers are then released by immersion in water and curl due to the stress distribution. Final structures resemble the shape of a spheroid or the Venus flytrap. Scale bar is 200 μm .

feet per minute) and crosslinked as spheres in the cationic bath, thus forming magnetic microbeads (diameters in the range of 10-100 μm). The so formed magnetic beads were rinsed extensively in deionized water and stored until use.

C. Experimental Setup

The system consists of eight stationary electromagnets with soft magnetic cores and is capable of producing magnetic fields and gradients up to 50 mT and 0.5 T/m at frequencies up to 100 Hz. For visual tracking, a Leica M80 microscope at 6.0 X magnification observes the workspace from above. We mounted a NIR laser (wavelength 785 nm, 1.5 W power, laser spot 5 mm, SLOC lasers, China) in a configuration that allows us to focus the laser beam directly onto the sample and effectively stimulate the light responsive bilayers.

D. Laser Excitation

The photothermal actuation of the hydrogel nanocomposites and the bilayers was tested using a focused NIR laser (wavelength 785 nm, 1.5 W power, laser spot 5 mm, SLOC lasers, China). Heating of the samples related to time of irradiation was monitored by means of a thermal camera

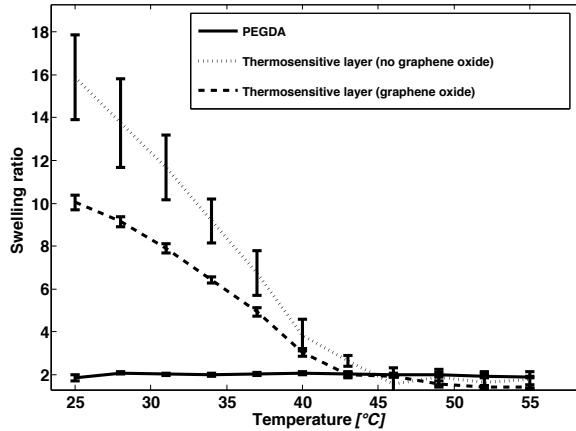


Fig. 4. Temperature dependent swelling ratio analysis of the individual hydrogel layers

(Flir, USA). An estimation of the average exposition time, and power was in this way established.

III. RESULTS AND DISCUSSION

The light responsive hydrogel bilayers are created to protect the payload from adverse effects (i.e. foreign body reactions) while providing a remotely controlled actuation for delivery. Alginate magnetic microbeads can be loaded with cells and drugs and at the same time provide the way to magnetically manipulate the full devices. The fabrication method consists of an easy and reliable double step process which is compatible with a huge variety of materials, allowing further combinations and solutions for the hydrogel bilayer production. We designed structures that could ensure a closed compartment where the beads could be accommodated in different configurations. The spheroid was created from a symmetrical 8 arms 2D star, while the Venus flytrap is the result of an elongated version of the previous design (see Figure 3d).

The final curvature ($1/\rho$ where ρ is the radius of curvature) of the devices can be modeled using from the Timoshenko formula for the bending of bilayers (equation 1):

$$\frac{1}{\rho} = \frac{6(\varepsilon_2 - \varepsilon_1)(1+m)^2}{h(3(1+m)^2 + (1+mn)(m^2 + \frac{1}{mn}))} \quad (1)$$

Where $n = E_1/E_2$, $m = a_1/a_2$, E_x is the elasticity modulus, a_x is the thickness of the layer, h is the total thickness, and ε_x is the strain of the film. The radius of curvature is mainly controlled by the difference in the strains of the films, which is related to the swelling ratios and their thickness. This dependence allowed us to control the final shape during the synthesis of the materials and the photolithography process.

A. Characterization of Swelling ratio and Transition Temperature

The functional characterization of the swelling ratio and transition temperature of the used hydrogels was determined

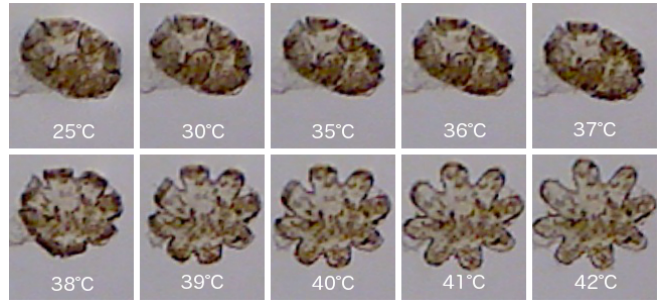


Fig. 5. Temperature response of self-folding soft microrobots.

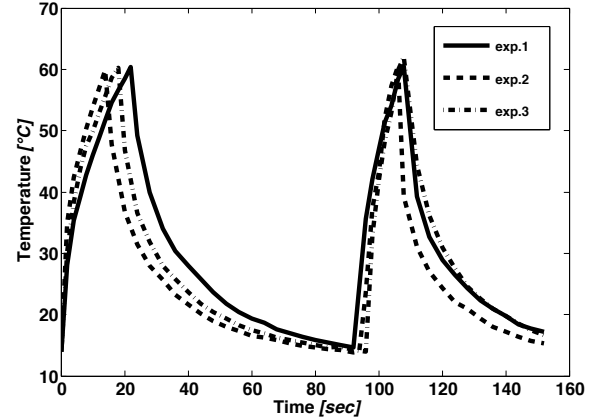
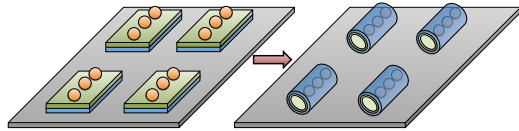


Fig. 6. NIR light sensitivity of the actuating layer. Three different samples were stimulated for two cycles till 60 °C to prove the repeatability of the mechanism.

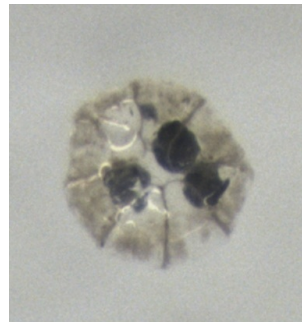
gravimetrically by using gel discs (diameter 4.5 mm, thickness 2 mm) produced by UV polymerization. The gels were allowed to swell at different temperatures (from 25°C to 55°C), in water bath (Julabo, Germany) and their equilibrium swelling ratio calculated at each temperature (Equation 2):

$$ESR = \frac{M_s - M_d}{M_d} \quad (2)$$

where M_s and M_d are the mass of the swollen hydrogel and the dried mass, respectively. They were measured using a precise weighing scale. The effect of graphene oxide on the swelling properties was investigated by means of the same method. The thermoresponsive nanocomposite (active layer) was synthesized starting from NIPAAm, a polymer naturally collapsing over its lower critical solution temperature (LCST, 32°C). By polymerizing it together with a hydrophilic comonomer like AAm, and a low concentration of crosslinker (PEGDA), we were able to increase the temperature of transition to a value of 40°C (see Figure 4), and at the same time provide a high swelling capability to the actuating layer. The inclusion of graphene oxide, though modifying significantly this parameter, did not influence the temperature of transition. Although tested with larger structures, the absolute values of swelling constitute an intrinsic property of the material and does not change with the size. Smaller sizes allow faster diffusion and therefore faster actuation of the devices.



(a) The beads were randomly distributed over open structures at high temperatures. The successive cooling and folding of the devices resulted in the final platform



(b) Final platform

Fig. 7. Loading mechanism of microbeads into hydrogel bilayers

A visual analysis of the folding/unfolding of the hydrogel bilayers was conducted by means of a USB digital microcamera (Dnt GmbH, Germany), using a custom made temperature controlled microchamber. The structures maintained a closed configuration till a value of 38-39°C (see Figure 5), thus potentially allowing navigation without loss of materials in a physiological human body environment.

NIR laser light sensitivity, provided by the inclusion of graphene oxide was tested by direct short exposure to a laser beam, focused at 785 nm (1.5 W power). As it can be seen in Figure 6, a temperature higher than 50°C is reached in the range of 10 seconds; the process appears repeatable even for continuous cycles of irradiation.

B. Bead Loading, Magnetic Manipulation, IR Release

The magnetic alginate microparticles were loaded inside the sealed compartments of the folded bilayers by mixing the two components in water at temperature higher than 40°C. The subsequent cooling allowed the hydrogel bilayers to close and entrapped the beads inside (Figure 7). Structures mimicking the Venus flytraps were able to create an ordered distribution of the beads along their main axis, thus having a more defined magnetic axis, while star like structures encapsulated the beads with no preferential order.

Magnetic manipulation of the final platform was achieved using a 5-DOF electromagnetic manipulation system, Octomag [9]. We demonstrated real-time, closed-loop servoing of individual magnetic alginate beads by implementing a proportional controller. The visual tracker was able to recognize the microrobot (see blue frame in Figure 8); the controller applied the required magnetic gradients to move the bead along the pre-planned circular trajectory (red circles in Figure 8 indicate the target waypoints). A short exposure to NIR excitation caused a rapid unfolding of the bilayer. Magnetic stimulation was then used to move the beads out of their

confined spaces (Figure 9).

C. Drug Delivery Tests

Delivery studies of brilliant green (BG), a dye used as a drug model, embedded into the nanocomposites, were performed to investigate the effect of laser exposure on the kinetics of drug release. Hydrogel disks similar as the ones used for the material characterization, were immersed into a 1 mM brilliant green (BG, Sigma Aldrich) solution in PBS. After 24 hours, they were rinsed briefly with water and divided in two classes. The first set of samples was allowed to release the dye in PBS (1 ml volume, exchanged at defined time intervals, to mimic the perfect sink condition), and the drug profile was defined by measurements of UV/VIS spectroscopy (Infinite M200 Pro, Tecan Ag, Switzerland) at 624 nm wavelength.

Similarly a set of three samples was exposed for the first hour of release to ON-OFF cycles (irradiation time=10 minutes, rest cycle=10 minutes) of NIR laser. One sample was continuously exposed for the first hour. Their drug release was evaluated in the same way as the control group. A similar experiment was conducted on hydrogel bilayers, to analyze the effect of the change of conformation (from closed tubule to open square) on the drug release profile.

The typical diffusion driven kinetics, following the Peppas-Korsmeyer model (equation 3, where $M(t)$ is the mass released at time t , and M_∞ is total mass) was slightly modified by an ON-OFF laser exposure performed for the first hour of experiments. As it can be seen in Figure 10, the laser induced collapse of the matrix decreases the amount of drug release by the hydrogels, due to shrinkage in pore sizes. The effect is even more visible when the layers are continuously exposed to the beam, without allowing any swelling in the meanwhile.

$$\frac{M(t)}{M_\infty} = \alpha t^n \quad (3)$$

This remote control of the drug release is expected to have reversed effects when a change of shape (from folded to unfolded structure) is involved in the diffusion driven process. By laser driven unfolding of polymer bilayers, the area exposed to the solvent is expected to augment (from a closed to an open configuration), and therefore to induce an increase in the drug release. A detailed investigation is currently going on to test this hypothesis.

D. Cytotoxicity and Cell Encapsulation

To explore the potential of the platform, we have also tested the biocompatibility of the protecting hydrogel bilayers and successfully encapsulated live cells inside alginate microbeads. Hydrogel bilayers were rinsed and washed thoroughly in DI water until non signal from unreacted materials was detected by UV/VIS spectrophotometry. They were subsequently sterilized in ethanol and UV light and submerged in culture medium in a 6-well plate. After 24 hours of incubation, the gel conditioned medium was transferred to the cells (3T3 fibroblasts), in well plates. After an

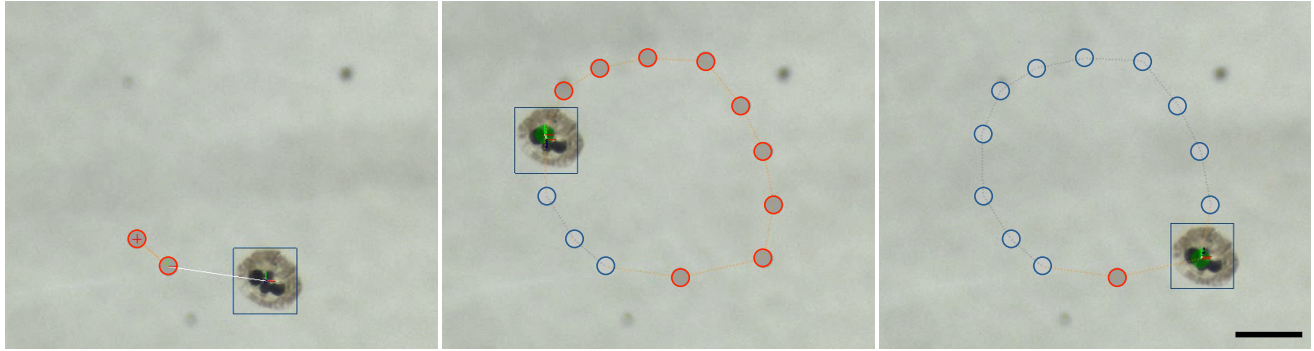


Fig. 8. Automated magnetic manipulation over a selected pattern. Real time optical tracking was used to maneuver the microrobots along planned trajectory. Red circles denote target destinations and the circles turn into blue as the robot passes over them. Scale bar is 500 μm .

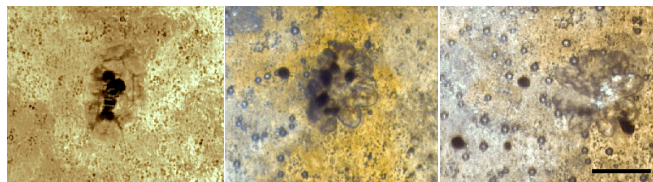


Fig. 9. Laser induced release of the beads from the hydrogel bilayers. A short exposure causes the unfolding of the bilayer. Magnetic stimulation is then used to move the beads out of their confined spaces. Scale bar is 500 μm .

incubation of 48 hours, WST-1 reagent (Roche) was added to each well. Three hours later, the solutions were analyzed at 435 nm to calculate the relative intensity of the absorbance compared to a control (no gel conditioned medium). Ten parallel experiments were conducted to evaluate the effect of the gels on cell proliferation. We did not observe any detectable change in cellular activity or a sign of toxic effect.

Cell encapsulation inside the magnetic alginate microbeads was performed during microbead fabrication. D1 mouse mesenchymal stem cells were rinsed three times and the culture medium was replaced with a 2.5% wt 4:1 LF10/60:LF 20/40 alginate, 100 mg/ml iron (II, III) oxide solution in PBS again through centrifugal washing. The mixture was nebulized over a calcium chloride bath and the formed beads rinsed three times in PBS and transferred in cultured medium. At one, three, seven days, LIVE/DEAD cell viability assays (Invitrogen, USA) were performed to assess the viability of D1 cells per microbead. Mesenchymal stem cells, encapsulated during the fabrication, were able to resist to the environment and proliferate in the subsequent week, without any negative effect of the surrounding hydrogel bilayers (see Figure 11).

E. Discussion

In this work, we presented the first prototype of a soft microrobotic platform to explore the potential of the system, and set milestones for further improvements. We fabricated our microgrippers with sizes slightly less than 500 μm using inexpensive materials such as foil masks, and microfabricated polymeric spacers. Using the same fabrication method with high-resolution chromium masks and metal spacers, scaling

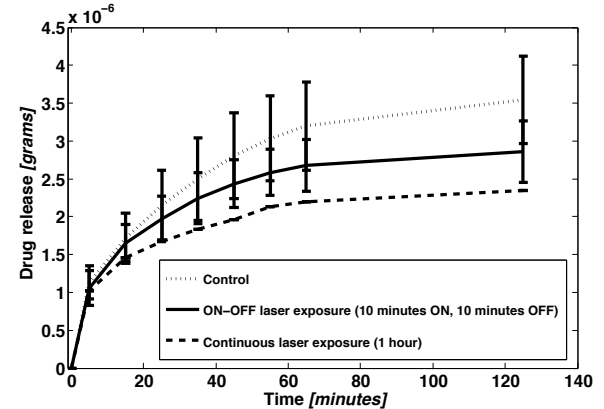


Fig. 10. Drug release studies performed on BG loaded active layers. The laser reduces the size of the samples influencing the pore size. The diffusion driven drug release is therefore lowered by ON-OFF cycles of exposure. The effect is even more visible when the samples are continuously exposed to the laser source.

down the size of self-folding devices 10-folds is straightforward [11]. As a result, we can scale the whole system (microgrippers along with trapped microbeads) down to 50 μm using already demonstrated fabrication techniques. They would be small enough to be navigated inside the arteries as demonstrated in [6].

Although reported as a preliminary study the photothermal actuation and its influence on drug release constitutes a novel investigation of the capabilities of the material. The idea of combining cell laden alginate magnetic microbeads inside a self-folding, protecting shell through self-assembly opens up new avenues of combining different functionalities in a single device.

A recent report showed that fully degradable polymer bilayers can be fabricated [12]. Our fabrication strategy is fully compatible with these biodegradable materials. The properties of PNIPAAm layers can be adjusted to introduce antifouling against cell and ECM protein adhesion [13]. Additional features can be introduced by studying the physical design of the device.

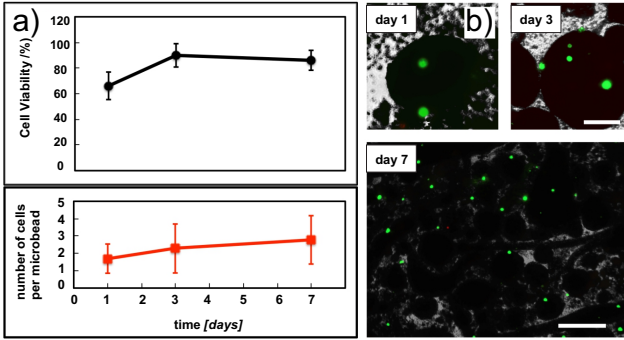


Fig. 11. Viability tests on stem cells encapsulated inside the magnetic alginate microbeads. A) The viability improves after the rough fabrication process, due to proliferation of the surviving cells. B) Fluorescence micrographs of live (green) versus dead (red) encapsulated cells. Scale bars are 200 and 500 μm respectively.

IV. CONCLUSIONS

Despite being developed as a prototype, the proposed microrobotic platform possesses most of the required features for minimally invasive therapies including 3D automated magnetic steering, the capacity to load and release drugs and biological entities, and remote control of the actuation. Moreover, the fabrication method is versatile and compatible with the production of even small devices, with different tailored materials. Visual tracking could be substituted by magnetic or NIR based strategies, allowing the use of these devices for *in vivo* applications.

V. ACKNOWLEDGMENTS

Financial support by the European Research Council Advanced Grant Microrobotics and Nanomedicine (BOTMED), by the ERC grant agreement n. 247283, and by the Swiss National Science Foundation are gratefully acknowledged. Additionally, this work was supported by the National Institutes of Health (R01 DE0013349). The authors are thankful to Prof. Dr. Christopher Hierold, and Prof. Dr. S. Pratsinis for their contribution and comments and to Dr. Simone Schurle for her help with magnetic manipulation experiments. The authors would also like to acknowledge Fabian Starsich and Rocco Bottani for their help during the work.

REFERENCES

- [1] B. J. Nelson, I. K. Kaliakatsos, and J. J. Abbott, "Microrobots for minimally invasive medicine," *Annual Review of Biomedical Engineering*, vol. 12, pp. 55–85, 2010.
- [2] A. Moglia, A. Menciassi, M. O. Schurr, and P. Dario, "Wireless capsule endoscopy: from diagnostic devices to multipurpose robotic systems," *Biomedical Microdevices*, vol. 9, pp. 235–243, 2007.
- [3] S. Yim and M. Sitti, "3-d localization method for a magnetically actuated soft capsule endoscope and its applications," *IEEE Transactions on Robotics*, 2013.
- [4] F. Ullrich, C. Bergeles, J. Pokki, O. Ergeneman, S. Erni, G. Chatzipiridis, S. Pane, C. Framme, and B. J. Nelson, "Mobility experiments with microrobots for minimally invasive intraocular surgery," *Investigative Ophthalmology and Visual Science*, vol. 54, pp. 2853–2863, 2013.
- [5] E. Gultepe, J. S. Randhawa, S. Kadam, S. Yamanaka, F. M. Selaru, E. J. Shin, A. N. Kalloo, and D. H. Gracias, "Biopsy with thermally-responsive untethered microtools," *Advanced Materials*, vol. 25, pp. 514–519, 2013.

- [6] P. Pouponneau, J. C. Leroux, G. Soulez, L. Gaboury, and S. Martel, "Co-encapsulation of magnetic nanoparticles and doxorubicin into biodegradable microcarriers for deep tissue targeting by vascular mri navigation," *Biomaterials*, vol. 32, pp. 3481–3486, 2011.
- [7] S. Pedron, S. van Lierop, P. Horstman, R. Penterman, D. J. Broer, and E. Peeters, "Stimuli responsive delivery vehicles for cardiac microtissue transplantation," *Advanced Functional Materials*, vol. 21, pp. 1624–1630, 2011.
- [8] T. S. Shim, S.-H. Kim, C.-J. Heo, H. C. Jeon, and S.-M. Yang, "Controlled origami folding of hydrogel bilayers with sustained reversibility for robust microcarriers," *Angewandte Chemie*, vol. 124, pp. 1449–1452, 2012.
- [9] M. P. Kummer, J. J. Abbott, B. E. Kratochvil, R. Borer, A. Sengul, and B. J. Nelson, "Octomag: An electromagnetic system for 5-dof wireless micromanipulation," *IEEE Transactions on Robotics*, vol. 26, no. 6, pp. 1606–1617, 2010.
- [10] C. Peters, S. Fusco, Y. Li, S. Kuhne, B. J. Nelson, and C. Hierold, "Backside liquid phase photolithography for fabricating self-organizing hydrogel bilayers," in *26th European Conference on Solid-State Transducers*, vol. 47, 2012, pp. 1219–1222.
- [11] J.-H. Cho, M. D. Keung, N. verellen, L. Lagae, V. V. Moshchalkov, P. V. Dorpe, and D. Gracias, "Nanoscale origami for 3d optics," *Small*, vol. 7, pp. 1943–1948, 2011.
- [12] S. Zakharchenko, E. Sperling, and L. Ionov, "Fully biodegradable self-rolled polymer tubes: a candidate for tissue engineering scaffolds," *Biomacromolecules*, vol. 12, pp. 2211–2215, 2011.
- [13] M. E. Nash, W. M. Carroll, P. J. Foley, G. Maguire, C. O'Connell, A. V. Gorelov, S. Beloshapkin, and Y. A. Rochev, "Ultra-thin spin coated crosslinkable hydrogels for use in cell sheet recovery-synthesis, characterization to application," *Soft Matter*, vol. 8, pp. 3889–3899, 2012.